# Flank collapse triggered by intrusion: the Canarian and Cape Verde Archipelagoes

Derek Elsworth [a,*], Simon J. Day [b,c]

[a] *Department of Energy and Geo-Environmental Engineering, Pennsylvania State University, University Park, PA 16802-5000, USA*
[b] *Department of Geography and Geology, Cheltenham and Gloucester College of Higher Education, UK*
[c] *Benfield Greig Hazard Research Centre, University College London, London, UK*

## Abstract

The potential to develop kilometer-scale instabilities on the flanks of intraplate volcanoes, typified by the Canary and Cape Verde Archipelagoes, is investigated. A primary triggering agent is forced injection of moderate-scale dikes, resulting in the concurrent development of mechanical and thermal fluid pressures along the basal décollement, and magmastatic pressures at the dike interface. These additive effects are shown capable of developing shallow-seated block instabilities for dike thicknesses of the order of 1 m, and horizontal lengths greater than about 1 km. For dikes that approach or penetrate the surface, and are greater in length than this threshold, the destabilizing influence of the magmastatic column is significant, and excess pore fluid pressures may not be necessary to initiate failure. The potentially destabilized block geometry changes from a flank-surface-parallel sliver for short dikes, to a deeper and less stable décollement as dike horizontal length builds and the effects of block lateral restraint diminish. For intrusions longer than about 1 km, the critical basal décollement dives below the water table and utilizes the complementary destabilizing influences of pore fluid pressures and magma ''push'' at the rear block-scarp. In addition to verifying the plausibility of suprahydrostatic pressures as capable of triggering failure on these volcanoes, timing of the onset of maximum instability may also be tracked. For events within the Cumbre Vieja (1949) and Fogo (1951, 1995) pre-effusive episodes, the observation of seismic activity within the first 1 week to 4 months is consistent with the predictions of thermal and mechanical pressurization. © 1999 Elsevier Science B.V. All rights reserved.

*Keywords:* aquathermal; poromechanics; flank instability; Fogo; Cumbre Vieja

## 1. Introduction

Large scale lateral collapses, with volumes of up to thousands of cubic kilometers, are a ubiquitous feature of oceanic island volcanoes in their most active, *shield-building*, stage of growth (e.g., Moore, 1964; Moore and Fiske, 1969). The overall slopes of these volcanoes vary in angle from less than 8° to more than 20°. At the lower end of this range, in particular, the causes of these massive failures are enigmatic (Iverson, 1991, 1992; Voight and Elsworth, 1992) since the destabilizing gravitational stresses generated on basal failure planes are much less than resisting frictional forces, for reasonable values of friction coefficients.

Models for the kinematics of preserved gravitational slumps assumed typical for oceanic volcanoes, including the Hilina slide system in Hawaii (Swan-

---
* Corresponding author. Tel.: +1-814-863-1643; fax: +1-814-865-3248; E-mail: elsworth@psu.edu

son et al., 1976; Ando, 1979; Buchanan-Banks, 1987; Lipman et al., 1985), are difficult to justify as the initial geometries of catastrophic long-runout slides, since motion must occur *updip* on landward dipping interfaces. Slides must initiate on primarily seaward dipping interfaces if sufficient momentum is to be generated for long-runout avalanches. In addition to the well-known occurrences of such deposits around the Hawaiian Islands, long-runout debris avalanche deposits have been observed on the ocean floor surrounding the Canarian Archipelago (Holcomb and Searle, 1993; Masson, 1996; Teide-Group, 1997; Urgeles et al., 1997), together with aborted collapse structures on the flanks of El Hierro (Day et al., 1997), and incipient collapse structures on Cumbre Vieja (La Palma) and Fogo in the Cape Verde Islands (see Day et al., 1999a-this volume). Indications of the importance of including pore fluid pressure effects in analysis of the stability of these steep-sided oceanic island volcanoes can be found in the patterns of flank deformation associated with certain recent eruptions. These are the 1949 eruption of the Cumbre Vieja volcano, La Palma (Canary Islands) (Day et al., 1999a-this volume); the 1951 eruption on Fogo (Cape Verde Islands) (Day et al., 1999b-this volume); and possibly also the 1995 eruption of Fogo (Heleno da Silva et al., 1999).

Flank failure is only feasible if processes are capable of significantly increasing destabilizing forces, or reducing strength of a décollement. Alternate mechanisms to describe mechanistic triggers for shallow debris avalanches include consideration of fluid pressurization resulting from lava accretion, surface saturation by rainfall (Iverson, 1996) or the presence of a soft underlying basement (Clague and Denlinger, 1994). Although plausible, the first set of triggers are rejected by Iverson (1996) as insufficiently strong. The presence of an extensive underlying magmatic plumbing system appears plausible, although it is applied (Clague and Denlinger, 1994) to the landward-dipping geometry of the Hilina (Kilauea) slide, and therefore is classified as kinematically incapable of developing into an avalanche. This mechanism also implies that deformation should continue between eruptions; although this is the case in Hawaii, Fogo and Cumbre Vieja show little evidence of deformation in inter-eruptive periods, but significant deformation in eruptive periods, as dis-

cussed below. An alternative, that could reduce strength sufficiently, is mechanical and thermal pore-fluid pressurization (Elsworth and Voight, 1995, 1996; Day, 1996; Voight and Elsworth, 1997; Hürlimann et al., 1997; van Wyk de Vries and Francis, 1997). According to these models, instability may be triggered by a reduction in strength on the décollement through an increase in pore fluid pressures in the volcanic edifice.

Here, we consider how a relatively small volume of magma, emplaced as dikes in a volcanic rift zone, can destabilize the edifice through the mechanical or thermal pressurization of pore fluids.

## 2. Field evidence for magmagenic fluid pressures

These postulated pressurization mechanisms have been observed. Mechanical pressurization has been observed in a series of intrusive events at Krafla, Iceland, with pore pressures rapidly reaching 70 m of water-head in a confined aquifer 4.3 km from the intrusion site (Brandsdóttir and Einarsson, 1979; Tryggvason, 1980; Stefánsson, 1981). Similarly, thermal pressurization is likely the cause of long-term anomalous flow from a borehole observed during the eruption of Heimaey (Björnsson et al., 1977). These processes of generating excess fluid pressures are not limited to mid-ocean ridge environments, with at least one example reported for island-arc volcanics (Watanabe, 1983). The potential to overpressurize rocks within the core of a volcanic edifice appears clear from these observed occurrences, and it is possible to match response directly through appropriate mechanistic models of static (Sigurdsson, 1982) and migrating (Elsworth and Voight, 1992) intrusions.

Paleo-evidence for aquathermal pressurization by dikes is present in the exhumed oceanic island Seamount Series in the Barranco de Las Angustias, La Palma (Staudigel, 1997). These rocks were uplifted above sea level and deeply incised both before and after the growth of overlying subaerial volcanic rocks, resulting in exposures of pillow lavas cut by an intense dike swarm. Both intrusive and extrusive rocks were affected by contemporaneous hydrothermal activity. Pipe-like zones of hydrothermal mineral (mainly zeolite)-cemented breccia along dike mar-
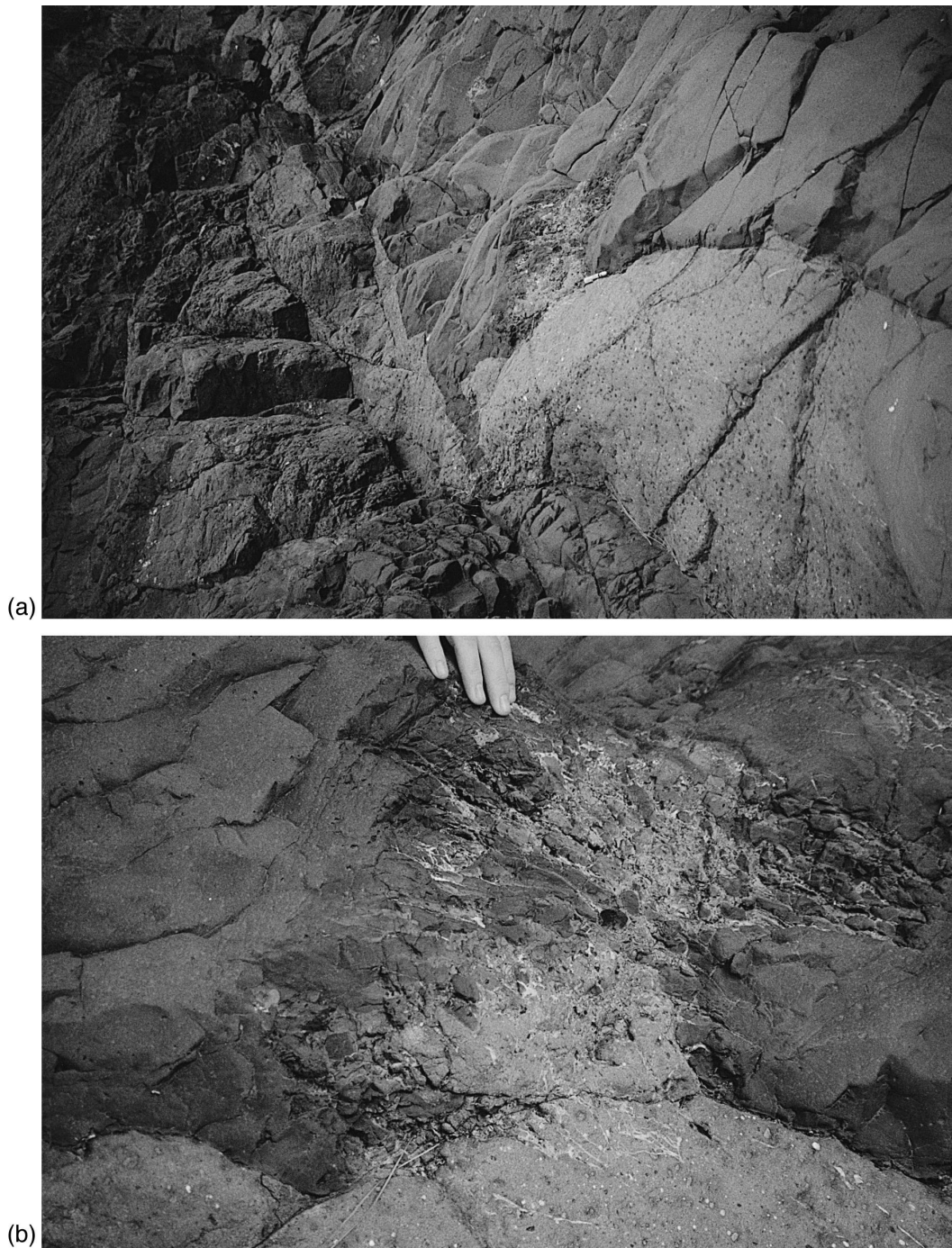
Fig. 1. (a) Irregular western margin of N–S-trending aphyric dike with intrusive horn structure and irregular breccia zone (extending to right of picture) at contact in centre of field of view. Host rock is older, altered olivine–phyric basaltic dike rock. Thickness of main breccia body ca. 30 cm: pen in centre of field of view is ca. 15 cm long. (b) Detail of main breccia zone showing zeolitic veining of host rock and brecciated mass of strongly chilled aphyric basalt dike rock. Note irregular, sharply-defined chilled margin at left side of brecciated rock mass.

gins result, typically at jogs and breached bridges in the dikes (Fig. 1a). The breccias cut both the host rocks and the broad, well-defined chilled margins (Fig. 1b) of the dikes. The brecciated dike rock contains a finely-divided hyaloclastic matrix in addition to the hydrothermal mineralization, suggesting that the brecciated zones formed soon after (but not during) dike emplacement. The explosive brecciation is driven by thermal fluid pressurization.

Although the example shown in Fig. 1 is from a submarine volcanic sequence, similar effects are possible below the water table in subaerial volcanoes. The geometry of the water table has been at least partly determined in a number of modern oceanic island volcanoes, including Kilauea in Hawaii (Thomas et al., 1983; Thomas, 1987), Tenerife (Anonymous, 1991) and El Hierro (Navarro and Soler, 1994) in the Canary Islands, Fogo in the Cape Verde islands (Bjelm and Svensson, 1982; Martins, 1988; Descloitres et al., 1995) and the Piton de la Fournaise volcano on Reunion (Coudray et al., 1990). The water table typically rises gradually from sea level at the coast, is moderately seaward-dipping between the coast and the major volcanic rift zones (which form the main topographic ridges) and central summit regions, and rises sharply within the main intrusion swarms to between 50% and 90% of the topographic elevation; water is perched and trapped between the dikes in the intrusion swarms. Despite jointing, dikes are generally impermeable, relative to the host volcanic rocks; they dominate the hydrology. On El Hierro, a single 6-m-thick dike impounds at least 70 m of water head (Soler, 1997). Dike swarms and intensely altered volcanic sequences in the walls of old, infilled collapse structures may combine to produce very high perched water tables such as that beneath the Cha das Caldeiras in Fogo (Bjelm and Svensson, 1982; Martins, 1988; Descloitres et al., 1995). A related phenomenon occurs where active rift zones occur on the flanks of older, higher structures and partially block the downslope flow within the edifice, such as the east rift of Kilauea, where water levels are 400 m higher than those on the southern side (Thomas, 1987; Jackson and Kauahikaua, 1987).

The presence of a largely saturated edifice is a necessary, but insufficient, precondition for the mechanical and aquathermal generation of pore pressures; their potential occurrence and influence are examined in the following.

## 3. Collapse mechanisms

Both mechanical and thermal fluid pressurization mechanisms may be quantified. Mechanical behavior is represented by a migrating volumetric dislocation (Cleary, 1977, 1978; Rudnicki, 1981; Elsworth, 1991), representing either the laterally or vertically migrating dike geometries illustrated in Fig. 2a, b. These represent observed intrusive modes for dike propagation during the shield-building phase. The development of lateral, rift-parallel intrusion within the volcanic pile is well documented for Kilauea volcano (Klein et al., 1987), where the asymmetric lateral stress regime favors this form (Rubin and Pollard, 1987). Vertical modes of propagation are reported for mid-oceanic ridge volcanoes in west (Gudmundsson et al., 1992) and central Iceland (Brandsdóttir and Einarsson, 1979; Tryggvason, 1980), in island-arc volcanoes (e.g., Mt. Unzen, Nakada et al., 1997) and for intraplate volcanoes in the Cumbre Vieja (La Palma) (Day et al., 1999a-this volume) and on Fogo (Day, 1996). Dike intrusion within predefined rifts in the upper 1 or 2 km may concurrently generate large ''uplift'' pore pressures and lateral tractions from magma ''push;'' these effects are additive.

The kinematics of the block is defined in Fig. 2c with the underlying detachment surface sloping seaward at angle $\alpha$, shallower than the edifice surface, $\beta$, and with the water table rising from sea level at an inclination, $\theta$. The crest of the rear scarp of the block is at elevation, $h_s$, above sea level, with this used as the principal length scale in normalizing other parameters. The ''daylighting'' toe of the failing block emerges at depth, $a$, below sea level. A dike of thickness, $w$, is intruded along the rear boundary of a potentially unstable flank block, of width, $d$, and at intrusion rate, $U$. Stability is influenced by the dike (horizontal) length, $d_m$, and height, $h_m$, that contacts the mobile block rear shown in Fig. 2a and b. This geometric terminology is used throughout, with thickness reserved to define the shortest dike dimension, $w$. Raw parameter magnitudes used in the analysis follow those of Table 1 in Elsworth and Voight (1995).
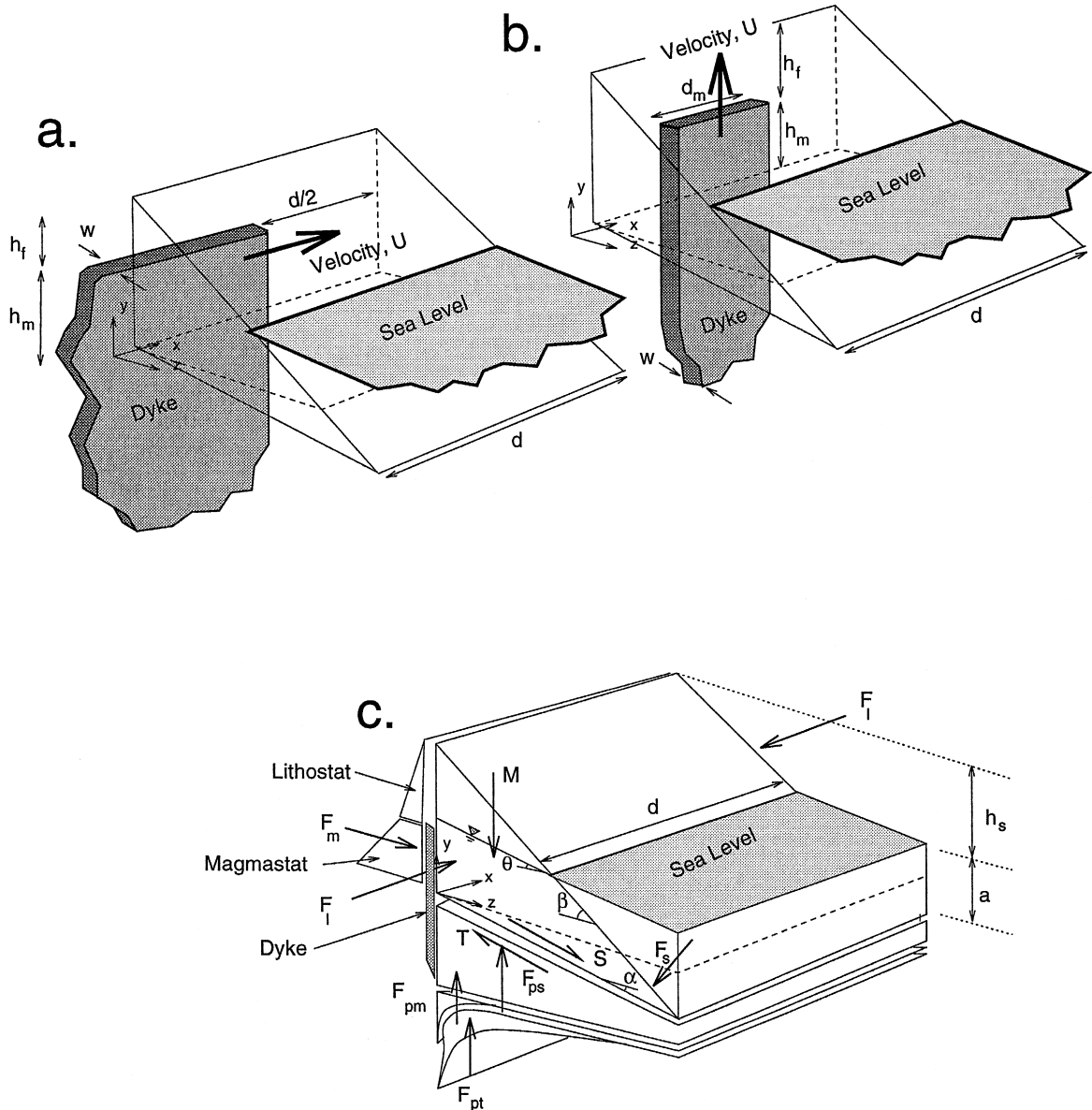
Fig. 2. Intrusion geometries within a volcano flank, illustrating (a) laterally mobile and (b) vertically mobile dikes, injected at emplacement velocity, $U$, and of thickness, $w$. Effective dike horizontal length, $d_m$ may be less than the width of the destabilized block, $d_D$. Dike depth is defined relative to the upper scarp surface as a freeboard height (height from dike crest to ground surface), $h_f$, leaving an effective magma column acting against the rear boundary of the block. From the emplacement geometry, the equivalent forces acting on a potential slide block may be determined. These include uplift due to groundwater pressures, $F_{ps}$, magmastatic loading at the rear block scarp, $F_m$, and destabilizing uplift forces due to mechanically, $F_{pm}$, and thermally, $F_{pt}$, induced pore fluid pressures.

## 3.1. Mechanical pressurization

Mechanically induced fluid pressures are controlled by intrusion rate, $U$, dike thickness, $w$, fluid permeability, $k$, and hydraulic diffusivity, $c$, of the host rock, or through the surrogate nondimensional groupings of intrusion velocity, $U_D$, and dike thickness, $w_D$. The non-dimensional fluid pressure gener-

ated by mechanical pressurization, $P_D^m$, is controlled as (Elsworth and Voight, 1995):

$$P_D^m = \mathscr{F}\left[ U_D, w_D, \text{geometry of failure surface}\right]. \quad (1)$$

Nondimensional parameters are defined as:

$$P_D^m = \frac{2\pi(p - p_s)}{Uw} \frac{k}{\mu}; \quad U_D = \frac{Uh_s}{2c};$$

$$w_D = \frac{\mu}{k} \frac{wc}{\pi \gamma_w h_s^2} \quad (2)$$

where $p - p_s$ is the fluid overpressure relative to ambient pressure, $p_s$, and $\mu$ and $\gamma_w$ represent the dynamic viscosity and unit weight of the fluid.

The model for mechanical pressurization directly follows that described in Elsworth and Voight (1995) except the boundaries of the finite dike are approximated. This is achieved by assuming an infinite dike to be intruded where the summation for fluid pressures is taken only over the effective dike horizontal length, $d_m$, and height, $h_m$ (Fig. 2). This approximation is reasonable, given the bounds on error in estimating mechanical properties.

### 3.2. Thermal pressurization

Thermally induced pore fluid pressures (Fig. 2) are modulated by the differential magma temperature, $\Delta T$, bulk skeletal modulus, $K_b$, and thermal expansion coefficient, $\alpha_t$, with migration rates of the pressure pulse controlled by thermal, $\kappa$, and fluid diffusivities, $c$. These parameters may be arranged into two unique nondimensional groupings, $A_D$ and $D$, and a diffusive time, $t_D$, to define thermal pressurization, $P_D^t$, following intrusion of a feeder dike. Correspondingly:

$$P_D^t = \mathscr{F}\left[ A_D, D, t_D, \text{geometry of failure surface}\right] \quad (3)$$

with individual parameters defined as:

$$P_D^t = \frac{(p - p_s)}{K_b \alpha_t \Delta T}; \quad A_D = \frac{AK_b D}{\gamma_w h_s}; \quad D = \sqrt{\frac{\kappa n}{c}};$$

$$t_D = \frac{4\kappa t}{h_s^2}. \quad (4)$$

Porosity of the intruded host, $n$, and time following emplacement, $t$, control behavior through the definition of these nondimensional parameters. Pa-

rameter ranges of $A_D$ and $D$ are selected from the material properties given in Table 1 of Elsworth and Voight (1995) and used in the evaluation of flank instability. The one-dimensional geometry of Delaney (1982) is used for the specific geometries of Fig. 2a and b. Intrusion-induced fluid pressures are summed over the base of the delineated block. For the vertically propagating dike, the one-dimensional pressure profile is integrated along the décollement and applied uniformly parallel to strike. For the laterally propagating dike, the pressure profile is integrated over the full décollement (Fig. 2a).

### 3.3. Stability model

Flank stability is determined by isolating a potentially unstable block as a simple free-body (Fig. 2c). Uplift fluid forces are evaluated, and used to resolve the translational equilibrium of the block where magmastatic pressures are applied at the block rear. The *factor of safety*, $F$, represents the ratio of forces resisting translational failure to those promoting failure. Where frictional resistance, alone, is assumed, the factor of safety may be divided by the friction coefficient for the flank material, $\tan\phi$, where values of $F/\tan\phi$ in the range 1–0.6 represent incipient failure for rocks of apparent frictional strengths typical to flank environments ($45° < \phi < 60°$).

## 4. Stability evaluation

Flank stability is evaluated for both vertically and laterally intruded dikes; mechanical and thermal effects are decoupled. Mechanical effects are typically short-lived, of the order of days (Elsworth and Voight, 1992), and thermal effects are more enduring and widespread. Since their mutually reinforcing effects are not evaluated, slopes will be less stable than calculated. A slope inclination of 24° and groundwater table inclination of 12° are used in the analyses.

### 4.1. Vertical dike propagation

The effects of pore fluid pressurization are examined for the geometry of Fig. 2b. The dike propa-

gates vertically with location defined by the depth of the dike front below the ground surface, $h_f$. Magmastatic pressures act over the portion of the dike in contact with the block rear, to a height of $h_m$, with the upper limit of magma pressure at the dike crest defined by the lithostat. Maximum fluid pressures are truncated at lithostatic.

### 4.1.1. Mechanical pressurization

The destabilizing effect of a vertically upwelling dike is illustrated in Fig. 3 for the geometry defined previously. For the 1-km-high rear scarp examined here, the magnitudes of dimensionless block width, $d_D$, effective dike height, $h_m$, and freeboard height (height from dike crest to ground surface) of magma

below the surface, $h_f$, scale directly to kilometers. Ranges of dimensionless dike thicknesses, $w_D$, represent minimum ($w_D < 10^{-1}$) and maximum ($w_D > 10^2$) reasonable mechanical events for dike thicknesses of the order of 1 m.

The destabilizing effects are important only for dikes greater than about 1 km in length; below this threshold, side restraint stabilizes the block. As the dike migrates higher in the edifice ($h_f \rightarrow 0$), stability diminishes. For a dike horizontal length of 1 km, the dike crest must approach the surface to initiate failure, with pore pressures providing an important destabilizing effect. For longer dikes, approaching 10 km in length ($d_m$), pore fluid pressurization does not appear necessary to initiate failure, although the
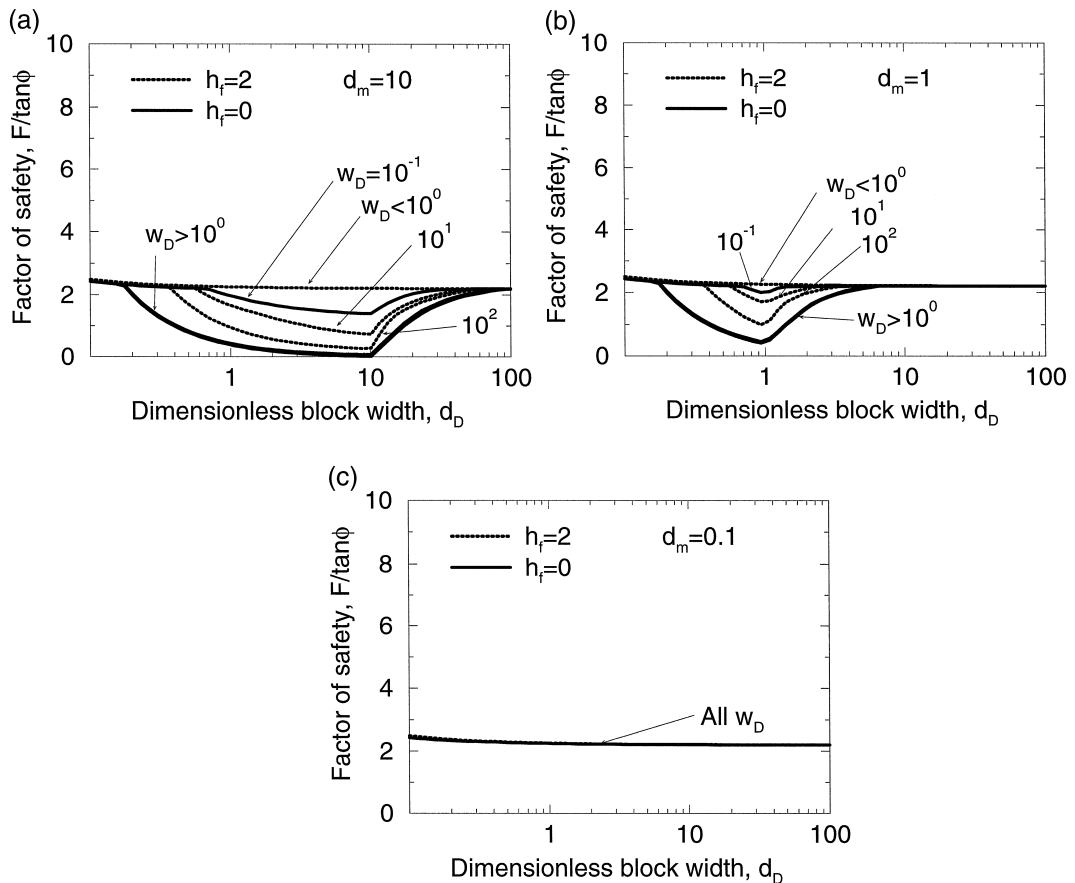


Fig. 3. The effects of dike horizontal length, $d_m$ of (a) 10, (b) 1, and (c) 0.1 km on flank stability for a 1-km-high flank crest dissected by a vertically upwelling dike at the rear, for $10^{-1} < w_D < 10^2$. Mechanical fluid pressurization effects only. Dike crest depth below the ground surface, $h_f$, as defined in Fig. 2(c). All lengths are normalized by volcano height above sea level, $h_s$.

presence of this effect may generate instability before magma ascent is complete; magmastatic forces are the dominant effect. For the longest intrusions, pore pressure magnitudes may reach lithostatic magnitudes, but with the minimum effect ($d_m = 10^{-1}$) inducing inconsequential fluid pressurization. For reasonable magnitudes of edifice strengths, flanks will be stable in the absence of ''magma push'' and fluid pressurization, as apparent from Fig. 3c.

Failure geometry also changes with dike length, thickness and location within the edifice. These effects are illustrated in Fig. 4 for an ascending dike at different ascent depths, $h_f$. The factor of safety reduces as the dike ascends (Fig. 4a); thicker dikes have the largest destabilizing effect, with pore pres-

sure effects felt for dikes as deep as 2 or 3 km (Fig. 4a). Pore pressures do not increase substantially with ascent, and stability remains constant until the intrusion approaches the surface, and the destabilizing effect of ''magma push'' is felt. The destabilizing effects of pore fluid pressurization and ''magma push'' are of the same order, and work additively, as apparent in Fig. 4a.

With dike ascent, the inclination of the critical basal plane rotates from near slope-parallel (Fig. 4b), where neither pore pressure or ''magma push'' effects are large, to a more shallow inclination, close to the inclination of the groundwater surface, as the intrusion approaches the surface. The ''daylighting'' toe moves up the submarine slope to close to sea
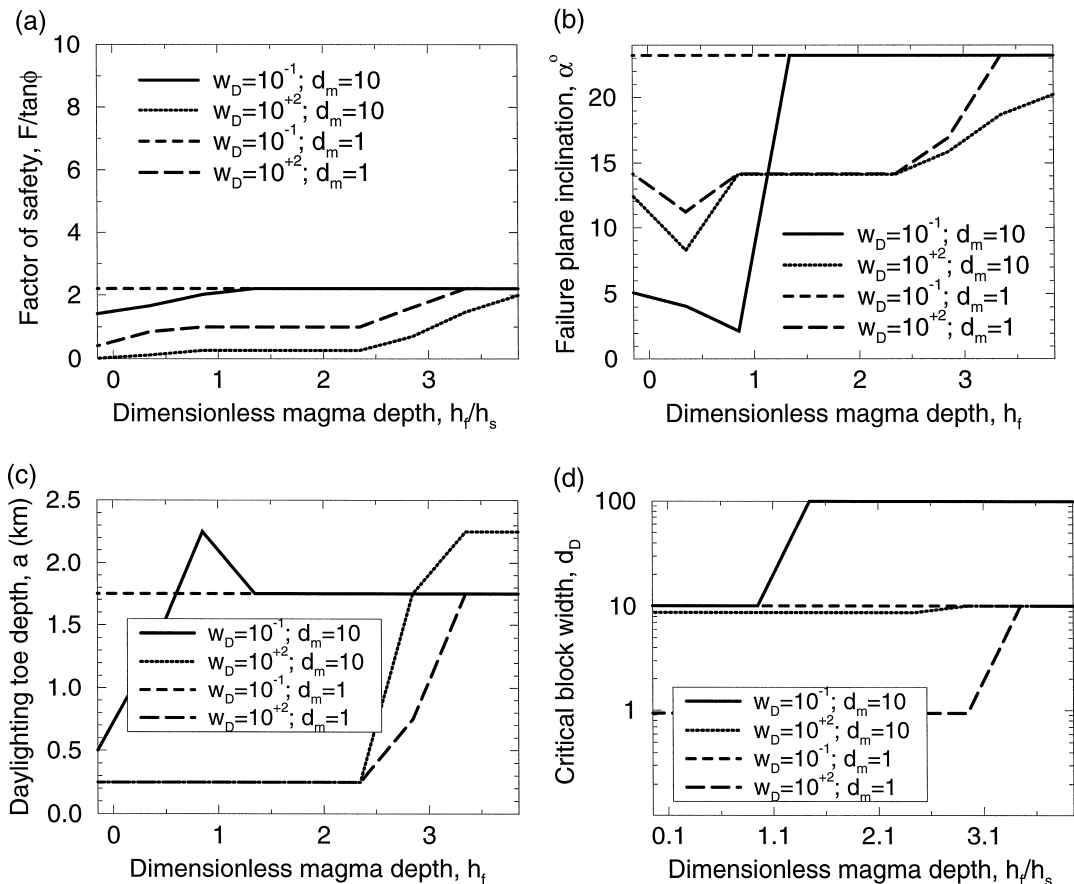


Fig. 4. Variation of (a) factor of safety, (b) critical failure plane inclination (degrees), (c) location of the ''daylighting'' toe [km], and (d) critical block width with magma depth below surface, $h_f/h_s$. Freeboard heights correspond, $h_f$, correspond to 0 through 4 km. Results are for mechanical pressurization effects and for the standard flank geometry with a 1-km scarp height above sea level. Selected horizontal dike lengths are 1 and 10 km. All lengths are normalized by volcano height above sea level, $h_s$.

level (Fig. 4c) as the dike reaches above the ground-water table. Where pore fluid pressurization or ''magma push'' are significant destabilizing agents, the critical block width is close to the dike length (Fig. 4d). For more stable configurations, unaffected by these agents, the critical failure geometry is the maximum considered block length, $d_D = 100$, as apparent in Fig. 4d.

### 4.1.2. Thermal pressurization

The destabilizing influence of thermally induced pore fluid pressures on the flank geometry of Fig. 2a are examined for intrusion lengths, $d_m$, of 10, 1 and 0.1 km in Fig. 5. Stability is referenced to time following instantaneous emplacement, with ranges of

mechanical and thermal parameters that yield alternately the minimum and maximum thermal destabilization.

For the maximum length dike, the behavior closely follows that of mechanical pressurization with zero freeboard height, $h_f$; pore fluid pressurization and ''magma push'' are both significant. These agents are especially important at later times, of the order of weeks to months, but may also influence behavior on shorter time scales. Again, the threshold for destabilization is a dike of 1 km length, although even for this critical length, the maximum thermal parameters are required; the minimum thermal parameters show no effect on stability. For the maximum thermal effect, destabilization increases monotonically with
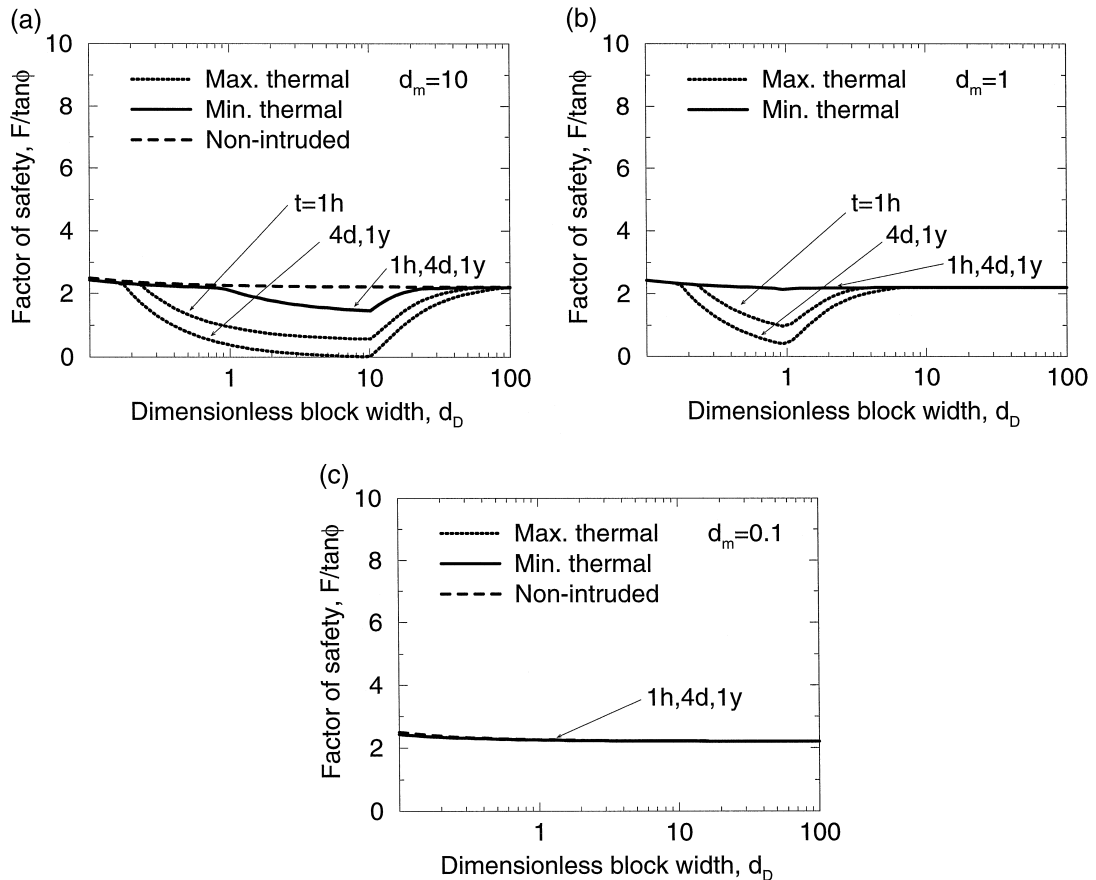


Fig. 5. The effects of dike horizontal lengths, $d_m$ of 10, 1, and 0.1 km on flank stability for a 1-km-high flank crest dissected by a vertically upwelling dike at the rear. Thermal fluid pressurization effects only. Dike is intruded to ground surface at time $t = 0$, with all times in hours [h], days [d], and years [y], relative to this instantaneous emplacement. Nominal dike lengths for a 1-km elevation rear scarp are (a) 10 km, (b) 1 km, and (c) 0.1 km.

time due to the continuous thermal output of the dike.

Fluid pressurization conditioned by the maximum thermal effect is an important destabilizing component; instability progresses with time (Fig. 6a). For the minimum thermal parameters, behavior is controlled by the invariant ''magma push'' geometry, resulting in shallow dipping critical failure surfaces (Fig. 6b) ''daylighting'' (Fig. 6c) at about 750 m below sea level. However, these geometries are not close to failure for any reasonable choice of strength parameters (Fig. 6c).

### 4.1.3. Deep failure and seismic instability

Deep seated failure may also result from mechanical or thermal pressurization effects, as illustrated for

orientations of the décollement that dip landward ($\alpha$ is negative), in Fig. 7. For mechanical pressurization, only magma upwelling close to the surface is sufficient to initiate failure at depth. This identifies the predominant influence of the magma column in inducing slip. For the particular dike length chosen in Fig. 7a mechanical pressures are necessary, in addition to the ''magma push'', to precipitate slip, at depth. Similarly, where thermal pressurization is considered (Fig. 7b), deep slip is also possible. Minimum stability, in these cases, is at the maximum dike length.

Although updip failure cannot precipitate long-runout slides for the deep geometry, it may clearly result in deep seated faulting and earthquakes, as is for example, characteristic of the Hilina fault system
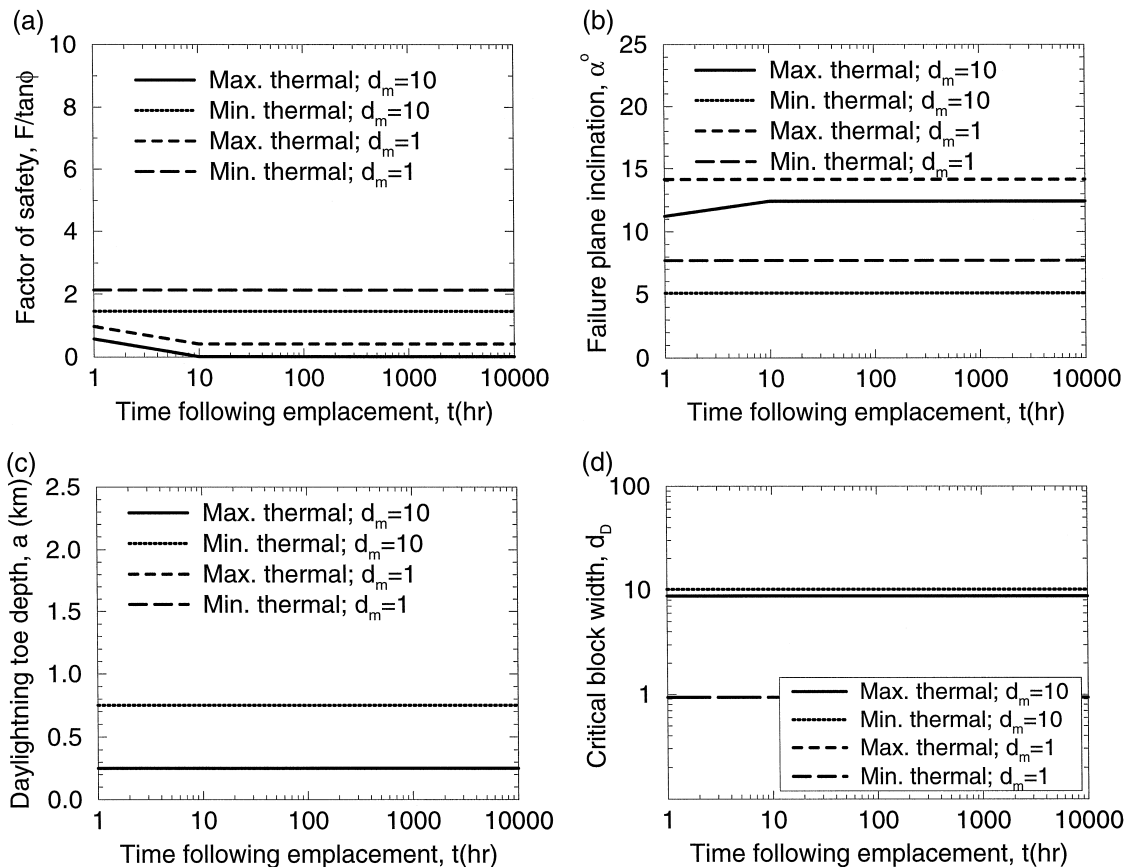


Fig. 6. Variation of (a) factor of safety, (b) critical failure plane inclination (degrees), (c) location of the ''daylighting'' toe [km], and (d) critical block width with time following magma emplacement, $t$. Results are for thermal pressurization effects and for the standard flank geometry with a 1-km scarp height above sea level. Selected intrusion lengths are 1 and 10 km. All lengths are normalized by volcano height above sea level, $h_s$.
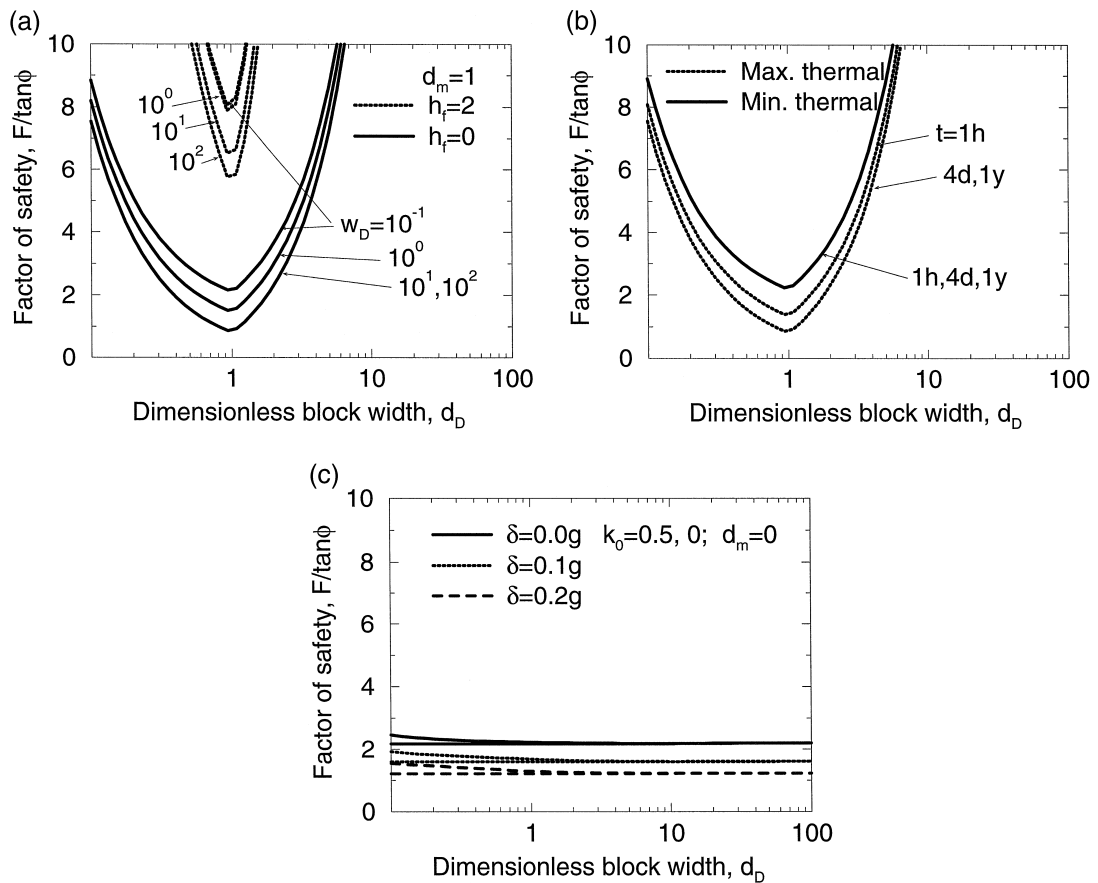
Fig. 7. Variation in factor of safety for deep-seated failures with landward dipping décollements resulting from (a) mechanical, (b) thermal pressurization mechanisms, and (c) the potential for inducing shallow flank failure in the absence of intrusional pore fluid pressurization and ''magma push'' due to lateral accelerations, $\delta$ defined in proportion to gravitational acceleration, $g$. Standard flank geometry with times relative to time of emplacement, given in hours [h], days [d], and years [y]. Dike length, $d_m$, is 1 km.

in Hawaii. Applied pseudo-static accelerations to a maximum of 0.2 g appear incapable of inducing significant shallow destabilization of long-runout slides in the absence of ''magma push'' (Fig. 7c).

### 4.2. Lateral dike propagation

The effects of fluid pressurization are *approximately* examined for the laterally propagating dike geometry of Fig. 2a.

#### 4.2.1. Mechanical pressurization

The assumed geometry includes the migrating dike front at the center of the failing flank block, enabling the full extent of the dislocation induced

pressure bulb to be contained within the failure plane. This will not yield the absolute minimum stability for the block, but this effect is overshadowed by the reduction in ''magma push.'' Correspondingly, the main difference between results for the vertically propagating dike (Fig. 3), and those for a laterally propagating dike, reported in Fig. 8, are the reduced destabilizing influence of the rear scarp magmastatic pressures.

The minimum and maximum mechanical effect for emplacement of a laterally migrating dike are shown in Fig. 8a–d, bracketing the response for lateral intrusions for reasonable ranges of dike thicknesses, $w_D$, and for normalized freeboard heights of $h_f/h_s = 0$, 0.5, 1.0 and 2.0. A minimum stability
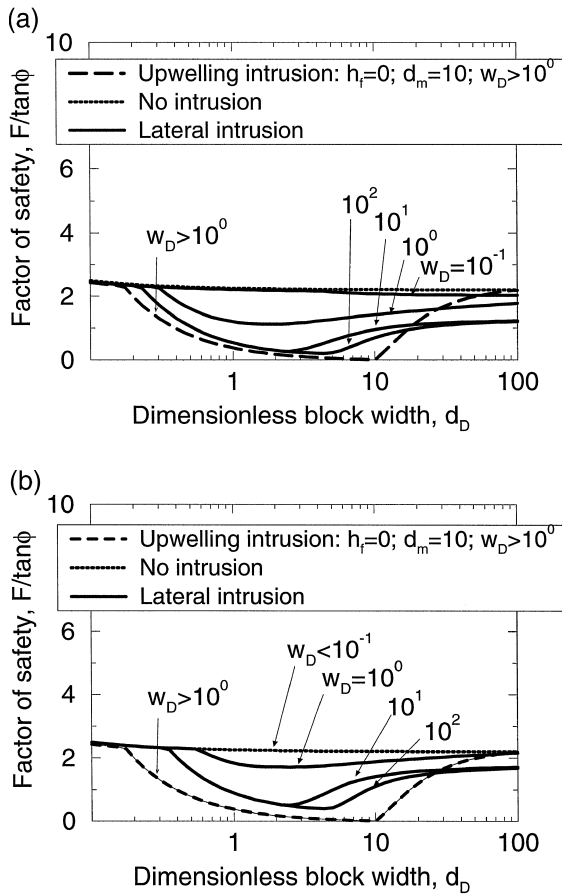
Fig. 8. Variation in stability for mechanical pressurization by a laterally propagating dike. Dike covers half the lateral width of potentially unstable block geometry. Results are for (a) a dike reaching the flank surface ($h_f = 0$), and (b) one present at a normalized freeboard height, $h_f / h_s$, of 2, below surface. These represent freeboard heights, $h_f$, of 0, and 2 km. Standard flank geometry.

exists where the uplift beneath the basal décollement is a maximum, before it proportionately diminishes as the block width grows. This form of theoretical response has been previously observed for laterally propagating dikes (Elsworth and Voight, 1995), and is consistent with the geometry used here, even as freeboard height, $h_f$, increases. Again, the intrusion of large thickness dikes is shown capable of destabilizing the standard flank geometry selected in this analysis, even for relatively deep intrusions, with $h_f / h_s = 2$. The correspondence between Fig. 8a and b, even for increasing intrusion depth, indicates that

magmastatic pressures do not significantly influence stability, as the critical failure décollement does not intersect the laterally propagating magma body. Critical dike lengths, of the order of 1 km are required for failure.

The morphology of the critical failure block changes with the length of the intruded dike. For dike lengths shorter than those required for the minimum slope factor of safety (i.e., about $d_D \approx 2$, or a block width of 2 km for the geometry of Fig. 8) the failure is shallow, and parallels the slope surface. The influence of fluid pressurization increases, as the dike length grows, driving the failure surface deeper; for the greatest dike lengths, the failure plane is deepest and consequently of shallowest inclination. For these examples, the dip magnitude and "daylighting" location (below sea level; defined as length $a$ in Fig. 2c) are defined for the pre-minimum (narrow failure), minimum (mid-length failure) and post-minimum (wide failure) failure modes. As the failing block widens, the critical failure surface changes from parallel to the ground-surface, to along the water table, to the most shallow inclination of 13°; these are for the narrow, medium and wide geometries, respectively. Similarly, toe "daylighting" depths increase from 250 m for the narrow and medium width blocks, to 500 m for the wide failure mode. This behavior confirms the potential increase in slide volume with increased dike length.

The deterioration of stability with "time following intrusion" is represented in Fig. 9a, for mechanical effects, and closely resembles the decrease in stability with increasing block length, identified in Fig. 8. For the chosen failure geometry with the dike-front centrally within the failing block, Fig. 8a may be converted to Fig. 9a through the relation $t = d_D h_s / 2U$; the height of the rear scarp above sea level is 1 km and intrusion velocity is 0.1 m/s. If the intrusion progresses at a rate an order of magnitude slower than this, the time scale on the figure must be multiplied by a factor of ten. The opposite is true for faster intrusion rates.

The potential to generate failure is controlled primarily by the severity of the intrusive event, as indexed by dike thickness, $w_D$. The time to failure is modulated by intrusion velocity; an ascending dike generates increasing downslope magmastatic force as it rises, acting against lateral restraint. Note that a
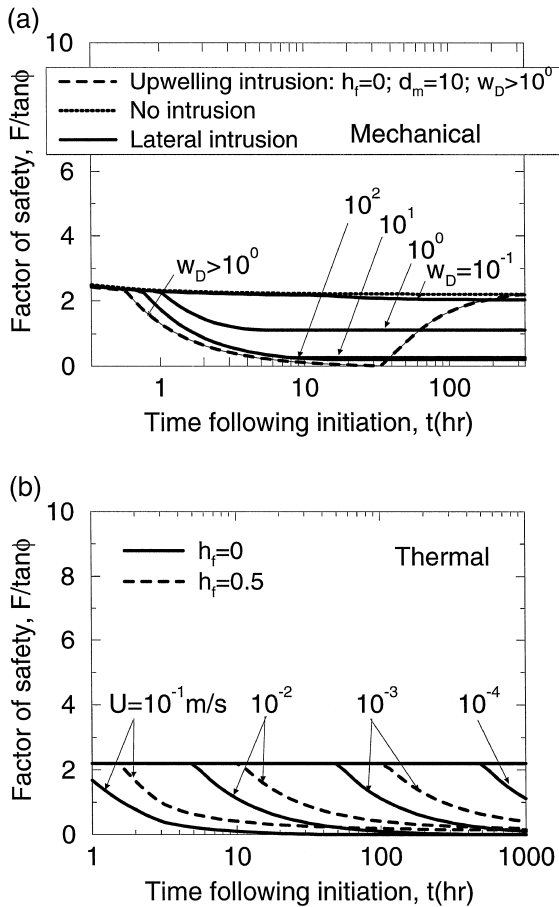
Fig. 9. Variation in stability with time for (a) mechanical and (b) thermal pressurization due to a laterally propagating intrusion. Mechanical behavior is for propagation at $10^{-1}$ m/s and is for an intrusion at surface, $h_f = 0$. Thermal pressurization is for lateral propagation both at (solid line) and below (dashed line) the surface. Intrusion rates, $U$, span $10^{-1}$ to $10^{-4}$ m/s. Standard flank geometry.

maximum potential failing block dimension will develop at the minimum factor of safety, and increased dike length will not increase this critical block dimension.

### 4.2.2. Thermal pressurization

The thermal response for a laterally propagating intrusion is similar to that for a vertically upwelling dike, as shown in Fig. 5. The critical block failure width closely matches effective dike horizontal length; as freeboard height increases, the influence of magmastatic pressure decreases. From the analyses

for upwelling behavior in Fig. 5, only the maximum thermal effect is capable of initiating instability. For short horizontal dikes, the destabilizing influence of both thermal pressurization and magmastatic forces, becomes trivial. Dike horizontal lengths of the order of 1 to 10 km appear necessary to initiate failure.

Stability may be followed in time, as shown in Fig. 9b. Intrusion rates of 0.1 to $10^{-4}$ m/s are incorporated, together with the maximum thermal effect. Time to potential failure is again modulated by the intrusion rate. Failure for the shallower intrusion occurs earlier due to the more rapid build-up of magmastatic forces acting at the rear scarp. Decreasing intrusion rates give a right shift to each graph by one order of magnitude in time. Time-to-failure varies directly with intrusion velocity, the ranges of 0.01 to 1 m/s being consistent with observed rates at Krafla of 0.5 m/s (Brandsdóttir and Einarsson, 1979; Tryggvason, 1980). These yield times to destabilization of between fractions of an hour to tens of hours.

Clearly, thermal effects appear of sufficient magnitude to initiate failure, given an appropriate combination of dike geometry, material parameters and intrusion rates.

## 5. Timing of destabilization in eruptions: an indicator of fluid pressurization mechanisms

In the absence of closely constrained parametric data, the stability analyses are most useful in defining important controlling parameters, modes of behavior, and in defining the time scales for hydrologic, seismic and geodetic monitoring. Mechanical pressurization effects are important during intrusion, and thermal effects are important during sustained eruption from fissures. In the absence of fortuitous corroborating fluid pressurization data, as present at Krafla (Brandsdóttir and Einarsson, 1979; Tryggvason, 1980), it is difficult to distinguish mechanical or thermal destabilization from the effects of seismic acceleration or magma ''push.''

Late-stage destabilization, unaccompanied by further dike emplacement, may have taken place during some recent eruptions; that of the Cumbre Vieja volcano on La Palma (Canary Islands) in 1949 (Pérez-Torrado et al., 1995; Day et al., 1999a-this volume, 1999b-this volume), and on Fogo, Cape

Verde Islands, in 1951 and possibly also in 1995. Geological evidence (Day et al., 1999a-this volume) indicates that the 20-km-long subaerial rift comprising the western flank of the Cumbre Vieja volcano, has become unstable in the last 7 ka. Similar evidence (Day et al., 1999b-this volume) indicates that a 10-km-wide section of the eastern flank of Fogo, has also become unstable, perhaps in the last three centuries. In both cases, reconfiguration of the volcanic rift zones preceded instability, enabling syn-eruptive seaward displacements along surface-rupturing fault systems during the 1949 and 1951 Cumbre Vieja events. Similar patterns of deformation are implied by recorded seismicity during the 1995 Fogo eruption. While relatively little is known about the subsurface geometry and the underlying mechanics of these episodes of deformation, their timing provides clues as to the most likely driving forces.

The 1949 eruption of La Palma began on June 24th, 1949 after a few days of felt precursory seismicity, and continued until sometime within the period July 30th–August 4th (Bonelli Rubio, 1950). It involved episodes of eruption from N–S fissures with a total length of about 1 km at the summit of the volcano (see map in Fig. 14 in Day et al., 1999a-this volume) between June 24th and 12th July, and again between July 30th and early August; and from downslope-trending fissures on the west flank of the volcano between 8th July and 26th July. The earlier stages of the eruption, in particular, were marked by vigorous but diffuse steam and $CO_2$-rich gas discharges along the crest of the Cumbre Vieja (Martin San Gil, 1960), indicative of heating of $CO_2$-charged groundwaters. The most intense seismicity felt during the eruption (there were no seismometers on the island) took place on July 1st and 2nd, about 1 week after the start of the eruption, and was not directly associated with formation or propagation of any eruptive fissures. Rather, the seismicity was associated with formation of a west-facing normal fault system, 3 km long at the surface and with a maximum offset at the surface of 4 m (Day et al., 1999a-this volume). There is no evidence (in the form of phreatic or fumarolic activity) to indicate that this faulting was associated with the emplacement of a near-surface dike. The seismicity was felt most intensely on the western side of the Cumbre Vieja suggesting that the surface fault rupture may

have been the surface expression of shallow faulting beneath this flank of the volcano.

The 1951 eruption on Fogo Island (Ribeiro, 1960) involved development of N–S-trending fissure vents in two segments north and south of the Pico do Fogo volcanic cone, which sits within the partly infilled, east-facing Monte Amarelo collapse structure (Day et al., 1999b-this volume). The segments were respectively 3 km and 2 km long, occupying almost the entire 9 km width (see map in Day et al., 1999b-this volume) of the Monte Amarelo collapse structure; the sidewalls acted as lateral boundaries to the incipiently unstable block. The near-surface dikes, bounding this collapse, occupied about 60% of the width of the back wall. Vents were emplaced at the extreme ends of the rifts at the start of the eruption on June 12th, and propagated along-rift between June 13th and June 28th (Ribeiro, 1960). Effusive activity subsequently diminished and ended around August 21st, with a swarm of earthquakes felt in eastern Fogo between August 12th and August 18th. At the same time (Day et al., 1999b-this volume), a number of dry fissure swarms ruptured the surface around the vents. These fissures are up to a meter or more wide and a few hundreds of meters long, with total swarm lengths up to 1 km, as illustrated in Fig. 10. There is no evidence of fumarolic activity nor of axial subsidence associated with these swarms (arguing against their formation by either emplacement or drainage of subsurface dikes), nor is there evidence for any vertical component of movement across them. They are therefore best interpreted as the product of eastward (seaward) sliding of the eastern flank of the section of Fogo within the Monte Amarelo collapse structure by a distance of the order of several meters.

The 1995 eruption of Fogo, although within the Monte Amarelo collapse structure, took place primarily on the WSW-trending volcanic rift zone of the volcano. However, where the main eruptive fissures (formed on April 2, 1995) intersected the region affected by the 1951 eruption, a north–south-trending secondary eruptive fissure formed on April 8, 1995 (Silveira et al., 1995). Excepting the first week, the seismicity of the 1995 eruption was recorded instrumentally (Heleno da Silva and Fonseca, 1998; Heleno da Silva et al., 1999-this volume). Whilst most of the seismic events recorded were relatively deep ($2 \rightarrow 8$ km depth) and aligned along

Fig. 10. View looking north along dry fissure swarm formed at the end of the 1951 eruption on Fogo. The nearest fissures are about 1 m across and cut deposits of the 1951 eruption from Monte Orlando (background, left) which are also draped over the vent of Monte Rendall (center) which was active only in the first phase of the 1951 eruption. The larger fissures cutting Monte Rendall may in part be associated with its collapse into lava flows from Monte Orlando but appear to be linked to the fissure system in the foreground.

the WSW rift zone, late stage eruptive events (June 1–July 31) were on shallow (less than 2 km depth) N–S- and NW–SE-trending structures in the regions affected by the 1951 activity; this likely signals a reactivation of weak structures formed in 1951 or earlier.

The principal episodes of flank instability-related seismic activity and surface deformation in these three eruptions were, therefore, delayed for significant periods after the starts of the eruptions: 1 week after the start of the 1949 Cumbre Vieja eruption; 2 months after the start of the 1951 Fogo eruption; and from 2 to 4 months after the start of the 1995 eruption. Furthermore, there is no evidence to indicate that these episodes were synchronous with, and directly related to, volcanic events such as further episodes of intrusion. The episodes of deformation are unlikely, therefore, to have been driven by an increase in ''magma push'' forces or by mechanical pressurization effects. They may, however, have been associated with thermal pressurization effects: the model results presented previously (Fig. 9) predict maximum thermal pressurization effects on time-

scales of 100 to 10,000 h (4 days to 1 year) after initial intrusion emplacement. Processing of the seismic data from the 1995 eruption of Fogo is still in progress [S.I.N. Heleno da Silva, pers. commun.] and it may be possible to identify other features of this seismicity indicative of high pore fluid pressures in the source region.

## 6. Conclusions

The potential to initiate flank failure on intraplate volcanoes, as a result of moderate-sized magmatic intrusions, has been established. Generic geometries, representative of the Cumbre Vieja rift and Fogo volcano are selected, that incorporate the potential for lateral and vertical dike propagation within the upper portions of the volcanic pile, centered on remnant rift structures. Potentially destabilized blocks may be at the kilometer scale, or larger, consistent with rift delineated blocks observed at Cumbre Vieja, on the Island of La Palma and on Fogo. These dikes may be of the order of a meter in thickness, with

minimum horizontal lengths of the order of 1 km required for destabilization. Potentially large destabilizing effects are due to the development of suprahydrostatic water pressures resulting from concurrent mechanical and thermal effects, augmented by direct driving pressures from a magmastatic column. Although data defining material parameters for volcano flanks are rare, reasonable selection of elastic, thermal and fluid transport parameters yield substantial magnitudes of overpressurization.

Both mechanical and thermal pressurization mechanisms are shown capable of initiating massive slides, for surface or subsurface dike crests. In all cases, the minimum requisite dike horizontal length is of the order of a kilometer. For dikes of greater extent than this, that penetrate close to the surface, fluid overpressurization mechanisms are not necessary to trigger failure. For lateral magmatic injections that do not penetrate the surface, and for rising dikes, the evolving geometry of the failing block is largely controlled by the intruding magma geometry. At small dike lengths, the critical failure mode uses the steepest possible surface and is parallel to the flank, above the water table. As the dike ascends, or extends horizontally, the critical failure surface deepens and is affected by excess fluid pressures and magma "push" at the block rear. In this mode, the basal failure surface of the potentially mobilized block is deepest and of shallowest inclination. The critical block width is largely controlled by dike horizontal length, indicating the significant influence of magmastatic processes on the evolving failure.

Timing of the onset of maximum instability may also be tracked using these models. For events within the Cumbre Vieja (1949) and Fogo (1951, 1995) pre-effusive episodes, the observation of seismic activity within the first 1 week to 4 months is consistent with the predictions of mechanical, and especially thermal pressurization. However, exact timing is difficult to constrain because of the uncertainty of material parameters and the lack of control on the form and rate of the intrusive processes.

## Acknowledgements

## References

Ando, M., 1979. The Hawaii earthquake of November 29, 1975: low dip angle faulting due to forceful injection of magma. J. Geophys. Res. 84, 7611–7626.

Anonymous, 1991. Plan Hidrologico Insular de Tenerife. Publ. Excmo. Cabildo Consular de Tenerife, Santa Cruz de Tenerife.

Bjelm, L., Svensson, C., 1982. Geophysical investigation on Ilha do Fogo (including a proposed geothermal drilling program). Unpublished Report, University of Lund, Sweden.

Björnsson, A., Kristjánson, L., Johnson, H., 1977. Some observations of the Heimaey deep drill hole during the eruption of 1973. Jökul 26, 52–57.

Bonelli Rubio, J.M., 1950. Contribucion al estudio de la erupcion del Nambroque o San Juan (isla de La Palma), Contribution to the study of the eruption of Nambroque or San Juan (island of La Palma). Madrid, Instituto Geografico y Catastral, 25 pp.

Brandsdóttir, B., Einarsson, P., 1979. Seismic activity associated with the September 1977 deflation of the Krafla central volcano in north–eastern Iceland. J. Volcanol. Geotherm. Res. 6, 197–212.

Buchanan-Banks, J.M., 1987. Structural damage and ground failure from the November 16, 1983 Kaoiki earthquake, Island of Hawaii. In: Decker, R.W., Wright, T.L., Stauffer, P.H. (Eds.), Volcanism in Hawaii. U.S. Geol. Surv. Prof. Pap., Vol. 1350, pp. 1187–1195.

Clague, D.A., Denlinger, R.P., 1994. Role of olivine cumulates in destabilizing the flanks of Hawaiian volcanoes. Bull. Volcanol. 56, 425–434.

Cleary, M.P., 1977. Fundamental solutions for a fluid-saturated porous solid. Int. J. Solids Struct. 13, 785–806.

Cleary, M.P., 1978. Moving singularities in elasto-diffusive solids with application to fracture propagation. Int. J. Solids Struct. 14, 81–97.

Coudray, J., Mairine, P., Nicolini, E., Clerc, J.M., 1990. Approche Hydrogeologique. In: Lenat, J.F. (Ed.), Le Volcanisme de La Reunion. Publ. Centre de Recherches Volcanologiques, Clermont, Ferrand, France. pp. 307–356.

Day, S.J., 1996. Hydrothermal pore fluid pressure and the stability of porous, permeable volcanoes. In: McGuire, W.C., Jones, A.P., Neuberg, J. (Eds.), Volcano Instability on the Earth and Other Planets. Geol. Soc. London, Spec. Publ. No. 110, pp. 77–93.

Day, S.J., Carracedo, J.C., Guillou, H., 1997. Age and geometry of an aborted rift flank collapse: the San Andres fault system, El Hierro, Canary Islands. Geol. Mag. 134 (4), 523–537.

Day, S.J., Carracedo, J.C., Guillou, H., Gravestock, P., 1999a. Recent structural evolution of the Cumbre Vieja volcano, La Palma, Canary Islands: volcanic rift zone reconfiguration as a precursor to volcano flank instability? J. Volcanol. Geotherm. Res. 94, 135–167.

Day, S.J., Heleno da Silva, S.I.N., Fonseca, J.F.B.D., 1999b. A past giant lateral collapse and present-day flank instability of Fogo, Cape Verde islands. J. Volcanol. Geotherm. Res. 94, 191–218.

Delaney, P.T., 1982. Rapid intrusion of magma into wet rock: groundwater flow due to pore pressure increases. J. Geophys. Res. 87, 7739–7756.

Descloitres, M., Ritz, M., Mourgues, P., 1995. TDEM Soundings for locating aquifers inside the Caldeira of Fogo Active Volcano, Cape Verde Islands. Proceedings of the meeting of the Environmental and Engineering Geophysics Society European Section, Environmental and Engineering Geophysics, Torino, Italy, 25–27/9/1995, pp. 110–114.

Elsworth, D., 1991. Dislocation analysis of penetration in saturated porous media. J. Eng. Mech. Div. Am. Soc. Civ. Eng. 117 (2), 391–408.

Elsworth, D., Voight, B., 1992. Theory of dike intrusion in a saturated porous solid. J. Geophys. Res. 97, 9105–9117.

Elsworth, D., Voight, B., 1995. Dike intrusion as a trigger for large earthquakes and the failure of volcano flanks. J. Geophys. Res. 100 (B4), 6005–6024.

Elsworth, D., Voight, B., 1996. Evaluation of volcano flank instability triggered by dike intrusion. In: McGuire, W.C., Jones, A.P., Neuberg, J. (Eds.), Volcano Instability on the Earth and Other Planets. Geol. Soc. London, Spec. Publ. No. 110, pp. 45–53.

Gudmundsson, A., Oskarsson, N., Gronvold, K., 1992. The 1991 eruption of Hekla, Iceland. Bull. Volcanol. 54 (3), 238–248.

Heleno da Silva, S.I.N., Fonseca, J.F.B.D., 1998. A seismological investigation of the Fogo volcano, Cape Verde Islands: preliminary results. Volcanology and Seismology, in press.

Heleno da Silva, S.I.N., Day, S.J., Fonseca, J.F.B.D., 1999. Fogo Volcano, Cape Verde Islands: seismicity-derived constraints on the mechanism of the 1995 eruption. J. Volcanol. Geotherm. Res. 94, 219–231.

Holcomb, R.T., Searle, R.C., 1993. Large landslides from oceanic volcanoes. Mar. Geotechnol. 13, 19–32.

Hürlimann, M., Ledesma, A., Martí, J., 1997. Analysis of large landslides triggered by volcanic activity. Application to Tenerife (Canary Islands). In: Pawlowsky-Glahn, V. (Ed.), IAMG 1997: CIMNE, Barcelona, pp. 274–279.

Iverson, R.M., 1991. Failure and runout of giant landslides on Hawaiian volcanoes: cases of enigmatic mechanics? Geol. Soc. Am. Abstr. Programs 47, A125.

Iverson, R.M., 1992. Rigid-wedge models for metastable flanks of Hawaiian volcanoes (abstract). Eos Trans. AGU 73 (43), 505, Fall Meeting suppl.

Iverson, R.M., 1996. Can magma-injection and groundwater forces cause massive landslides on Hawaiian volcanoes? J. Volcanol. Geotherm. Res. 66, 295–308.

Jackson, D., Kauahikaua, J., 1987. Regional self-potential anomalies at Kilauea Volcano. In: Decker, R.W., Wright, T.L.,

Stauffer, P.H. (Eds.), Volcanism in Hawaii. U.S. Geol. Surv. Prof. Pap., Vol. 1350, pp. 947–959.

Klein, F.W., Koyanagi, R.Y., Nakata, J.S., Tanigawa, W.R., 1987. The seismicity of Kilauea's magma system. U.S. Geol. Surv. Prof. Pap. 1350, 1019–1085.

Lipman, P.W., Lockwood, J.P., Okamura, R.T., Swanson, D.A., Yamashita, K.M., 1985. Ground deformation associated with the 1975 magnitude 7.2 earthquake and resulting changes in activity of the Kilauea volcano, Hawaii. U.S. Geol. Surv. Prof. Pap. 1276, 45.

Martin San Gil, M., 1960. El Volcan de San Juan. Publ. Madrid.

Martins, V.C., 1988. Preliminary geothermal investigations in Cape Verde. Geothermics 17, 521–530.

Masson, D.G., 1996. Catastrophic collapse of the volcanic island of Hierro 15 Ka ago and the history of landslides in the Canary Islands. Geology 24 (3), 231–234.

Moore, J.G., 1964. Giant submarine landslides on the Hawaiian Ridge. U.S. Geol. Surv. Prof. Pap. 501 D, D95–D98.

Moore, J.G., Fiske, R.S., 1969. Volcanic substructure inferred from dredge samples and ocean-bottom photographs, Hawaii. Geol. Soc. Am. Bull. 80, 1191–1202.

Nakada, S., Eichelberger, J., Shimizu, H., 1997. Researchers discuss Mt. Unzen, a decade volcano. Eos 79 (45), 505–506.

Navarro, J.M., Soler, C., 1994. El Agua en El Hierro. Resumen del Avance del Plan Hidrologico de la Isla de El Hierro. Publ. Excmo. Cabildo Insular de El Hierro y Consejeria de Obras Publicas Vivienda y Agua, Santa Cruz de Tenerife. 59 pp.

Pérez-Torrado, F.J., Carracedo, J.C., Mangas, J., 1995. Geochronology and stratigraphy of the Roque Nublo Cycle, Gran Canaria, Canary Islands. J. Geol. Soc. London 152, 807–818.

Ribeiro, O., 1960. A Ilha do Fogo e as suas erupcoes (2nd edn.). (The island of Fogo and its eruptions) Memorias, serie geografica I. Publ. Junta de Investigacoes do Ultramar, Ministerio do Ultramar, Lisbon, Portugal.

Rubin, A.M., Pollard, D.D., 1987. Origins of blade-like dikes in volcanic rift zones. In: Decker, R.W., Wright, T.L., Stauffer, P.H. (Eds.), Volcanism in Hawaii. U.S. Geol. Surv. Prof. Pap., Vol. 1350, pp. 1449–1470.

Rudnicki, J.W., 1981. On fundamental solutions for a fluid-saturated porous solid. In: Cleary, M.P. (Ed.), Int. J. Solids Struct., Vol. 17, pp. 855–857.

Sigurdsson, O., 1982. Analysis of pressure pulses resulting from volcanic activity in the vicinity of a well. MS thesis, Univ. of Oklahoma, Norman, 72 pp.

Silveira, A.B., Serralheiro, A., Martins, I., Cruz, J., Madeira, J., Munha, J., Pena, J., Matias, L., Senos, M.L., 1995. A erupcao da Cha das Caldeiras (Ilha do Fogo) de 2 de Abril de 1995. Proteccao Civil 7, 3–14.

Soler, C., 1997. Abastecimiento General de El Hierro. Publ. y Consejeria de Obras Publicas Vivienda y Agua, Santa Cruz de Tenerife. 26 pp.

Staudigel, H., 1997. The Pliocene Seamount Series of La Palma: A field trip along the Barranco de Las Angustias, Proc. Int. Workshop on Volcanism and Volcanic Hazards in Immature Intraplate Oceanic Islands. Excursion Guidebook, 250 pp.

Stefánsson, V., 1981. The Krafla geothermal field, northern Ice-

land. In: Rybach, L., Muffler, L.J.P. (Eds.), Geothermal Systems; Principles and Case Histories. Wiley, New York, pp. 273–294.

Swanson, D.A., Duffield, W.A., Fiske, R.S., 1976. Displacement of the south flank of Kilauea Volcano: the result of forceful intrusion of magma into the rift zone. U.S. Geol. Surv. Prof. Pap. 963, 39.

Teide-Group, 1997. Morphometric interpretation of the northwest and southeast slopes of Tenerife, Canary Islands. J. Geophys. Res. 102 (B9), 20325–20342.

Thomas, D., 1987. A geochemical model of the Kilauea east rift zone. In: Decker, R.W., Wright, T.L., Stauffer, P.H. (Eds.), Volcanism in Hawaii. U.S. Geol. Surv. Prof. Pap., Vol. 1350, pp. 1507–1525.

Thomas, D.M. et al., 1983. Geothermal resources of Hawaii. Hawaii Institute of Geophysics Map. Publ. United States Government Printing Office.

Tryggvason, E., 1980. Subsidence events in the Krafla area, north Iceland, 1975–1979. J. Geophys. 47, 141–153.

Urgeles, R., Canals, M., Baraza, J., Alonso, B., Masson, D., 1997. The most recent megalandslides of the Canary Islands: El Golfo debris avalanche and Canary debris flow, west El Hierro Island. J. Geophys. Res. 102 (B9), 20305–20323.

van Wyk de Vries, B., Francis, P.W., 1997. Catastrophic collapse at stratovolcanoes induced by gradual volcano spreading. Nature 387, 387–390.

Voight, B., Elsworth, D., 1992. Resolution of mechanics problems for prodigious Hawaiian landslides: magmatic intrusions simultaneously increase driving force and reduce driving resistance by fluid pressure enhancement (abstract). Eos Trans. AGU 73 (43), 506, Fall Meeting suppl.

Voight, B., Elsworth, D., 1997. Failure of volcano slopes. Géotechnique 47 (1), 1–31.

Watanabe, H., 1983. Changes in water level and their implications to the 1977–1978 activity of Usu volcano. In: Shimozuru D., Yokoyama, J. (Eds.), Arc Volcanism: Physics and Tectonics. Terra Scientific, Tokyo, pp. 81–93.